Chloritization in Paleoproterozoic granite ore system at Malanjkhand, Central India: mineralogical studies and mineral fluid equilibria modelling

Dinesh Pandit*

National Centre for Antarctic and Océan Research, Goa 403 804, India

In the Malanjkhand Granitoid (MG), chlorite occurs in micro-domain along with mineral assemblage biotite, hornblende, quartz, K-feldspar and plagioclase. Chloritization of biotite is the most dominant processes during the hydrothermal alteration in MG ore system followed by alteration of hornblende. Chlorite composition revealed two major types of substitution mechanism, i.e. couples Tschermak (TK) and di-trioctahedral (DT) which correspond to the coupled exchange of Mg and Fe for Al between end-members clinoclore–daphanite and amesite. TK substitution is more prominent than DT substitution between end-members of chlorite solid solution during hydrothermal alteration in MG. Temperature estimates for chloritization using chlorite geothermometry range from 110°C to 400°C and are consistent with the temperature of hydrothermal mineralization (200–375°C) at Malanjkhand. The chloritization process incorporates K^+ and Ca^{2+} ions in the hydrothermal fluids. Therefore, it is inferred that the chloritization in granitic plutons is due to alteration of biotite and hornblende which increases the oxygen fugacity and activities of K^+ and Ca^{2+} ions in the hydrothermal fluid.

Keywords: Activity ratios, alteration, chloritization, granite, hydrothermal fluids.

CHLORITIZATION is defined as the process of formation of chlorite mainly due to hydrothermal alteration or metasomatic processes. It is a common product of hydrothermal alteration of primary ferromagnesian minerals like biotite, amphiboles, etc. in granitoids[1]. Biotite readily alters to chlorite at low–moderate temperatures, and the product is often present as a complex sandwich of chlorite layers coherently disposed between relic layers of biotite. The structural formula of chlorites consists of 2 : 1 : 1 layers, i.e. negatively charged 2 : 1 layers of ideal composition $[R^{2+},R^{3+}]_3(Si_{4-x}Al_x)O_{10}(OH)_2$ and positively charged interlayers $[R^{2+},R^{3+}]_3(OH)_6$ that alternate along the crystallographic *z*-direction[2,3]. Chlorites are hydrous silicate minerals, primarily incorporating Mg, Al and Fe in octahedral site and Al and Si in tetrahedral site; form a continuous solid solution series between Mg and Fe species[3]. The sheet structure of primary mica is relatively unchanged and immobile with addition of water during the hydrothermal alteration process. In fact, this process is more complex than understood earlier, and the behaviour of K^+, Na^+, Ca^{2+}, Mg^{2+}, Fe^{2+} and other ions needs to be addressed in greater detail.

Petrological and geochemical studies of Paleoproterozoic Malanjkhand hydrothermal system have revealed that there are systematic mineralogical and textural changes in the host granitoid rocks[4,5]. Hydrothermal alteration process is sluggish in nature and rapidly changes with the change in physical and chemical properties of the mineralizing ore fluids, but does not reach equilibrium conditions with the surrounding physico-chemical environment. In such cases, various intermediate mineral reactions have caused alteration of host rocks. They cause changes in the mineralogical and chemical composition of a rock and the resultant product is useful to constrain the physico-chemical conditions of hydrothermal alteration. Chemistry of secondary minerals can be used to identify, classify and characterize some important hydrothermal alteration processes in the mineralized Malanjkhand Granitoid (MG). In the present work, an attempt has been made to study the chloritization phenomenon and its role in hydrothermal/deuteric alteration process. For this purpose, rock samples were collected from the Malanjkhand mine pit and surrounding host granitoid rock. The main objective is to describe the chloritization phenomenon in granite ore system considering geological thermodynamic parameters.

Geological settings

The ENE–WSW trending Central Indian Tectonic Zone (CITZ) divides the peninsular India into two parallel structural domains (Figure 1 *a*): Son–Narmada (SONA) lineament represents the northern boundary, whereas

*e-mail: dpandit@hotmail.com

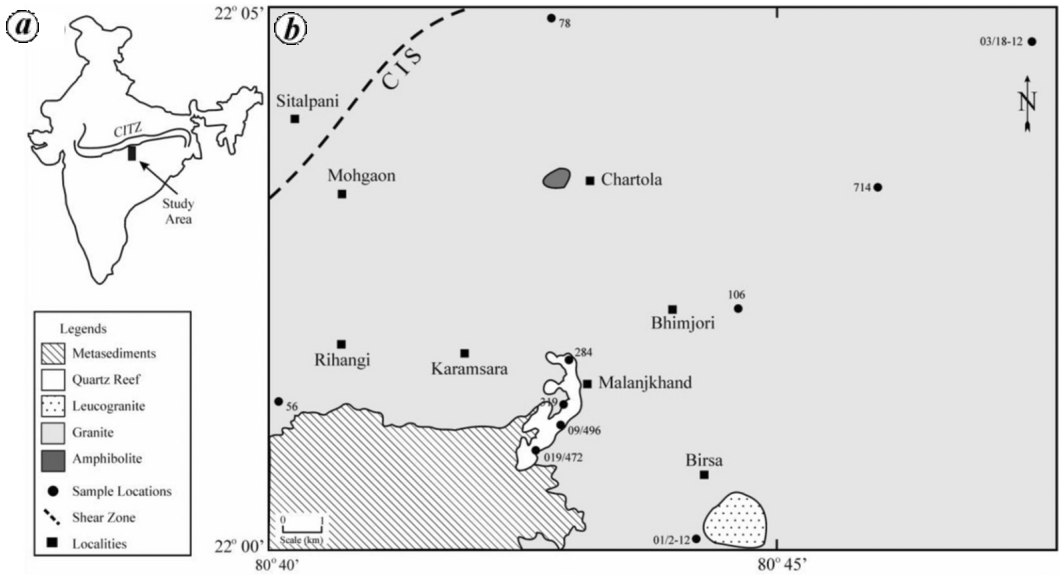

Figure 1. ***a***, Map of India showing location of the Malanjkhand Granitoid (MG) with respect to Central Indian Tectonic Zone (CITZ). ***b***, Geological map of Malanjkhand granitoid showing location of mineralized quartz reef. CIS represents the southern boundary of the CITZ.

Sausar Mobile Belt (SMB) defines the southern boundary[6,7]. The southern boundary of CITZ comprises of granulite belt with high strain ductile shear zone known as Central Indian Suture (CIS) trending ENE–WSW extending from southeast of Nagpur to south of Korba is ~ 500 km in length[8–10]. MG located adjacent to and south-southeast of CIS is exposed over an area of ~ 1400 km^2 and hosts one of the largest copper deposits of India (Figure 1 *b*). It is a coarse-grained granite–granodiorite, calc-alkaline with I-type affinity and is categorized as peraluminous[4]. It is dominated by pink granitoid in the mineralization zone because of conspicuous enrichment in K-feldspar which imparts pink colouration. The remaining part of the granitoid body shows grey colour[5]. The granitoids have yielded emplacement age ~ 2.48 Ga based on U/Pb SHRIMP RG dating of zircons[11], which is considered as a large single episode of granitic activity (Phase-I as MGC-I). Two subordinate bodies of leucogranite/microgranite with sporadic occurrences at Birsa and Devgaon village within the host MG[12] (D. Pandit, unpublished) are considered as the second episode of granitic activity (Phase-II as MGC-II). The leucogranite yielded an imprecise younger age ~ 2.1 Ga based on whole-rock Rb–Sr isochron[13]. Thus, the MG dominantly comprises of granitoid of two episodes of Paleoproterozoic granitic activity responsible for the formation of copper (+ molybdenum and gold) mineralization. Mineralized zone occurs in the form of an arcuate mineralized quartz reef of about 1.8 km strike length with N–S trend. Earlier workers report that the mineralized hydrothermal fluid evolved internally causing deuteric alterations with remobilization of various elements from the host rock and converged to a fracture zone that gave rise to the mineralized quartz reef[5,12]. In general, it represents a Paleoproterozoic granite ore system formed due to extensive hydrothermal alteration processes driven by internally evolved mineralizing ore fluids.

Petrography

The MG is dominantly biotite–hornblende-bearing quartzo–feldspathic rock. Major primary silicate minerals are quartz, plagioclase, K-feldspar, biotite, hornblende and epidote, whereas chlorite is present as the dominant secondary silicate mineral mostly in association with biotite and occasionally with hornblende. Petrographic photomicrographs from MG indicate that chlorite occurs in six micro-domains with altered mineral assemblages associated with partially chloritized biotite (Figure 2 *a*), partially chloritized biotite associated with K-feldspar present as inclusions (Figure 2 *b*), chlorite–biotite–quartz–plagioclase (Figure 2 *c*), massive grains of chlorite with biotite–plagioclase–quartz (Figure 2 *d*), partially chloritized hornblende and biotite (Figure 2 *e*) and fibrous aggregates of chlorite (Figure 2 *f*). Panigrahi *et al.*[5] also reported various textures of chlorite such as massive grains, mostly resulting from complete or partial chloritization of biotite, medium-size grains associated with magnetite, magnetite + pyrite or pyrite + chalcopyrite aggregates and extremely fine-grained aggregates associated with magnetite as well as interwoven chalcopyrite. Various textures formed because of chloritization at different stages of alteration in the Malanjkhand hydrothermal system. It indicates that there is a systematic mineralogical and textural changes in biotite and hornblende to

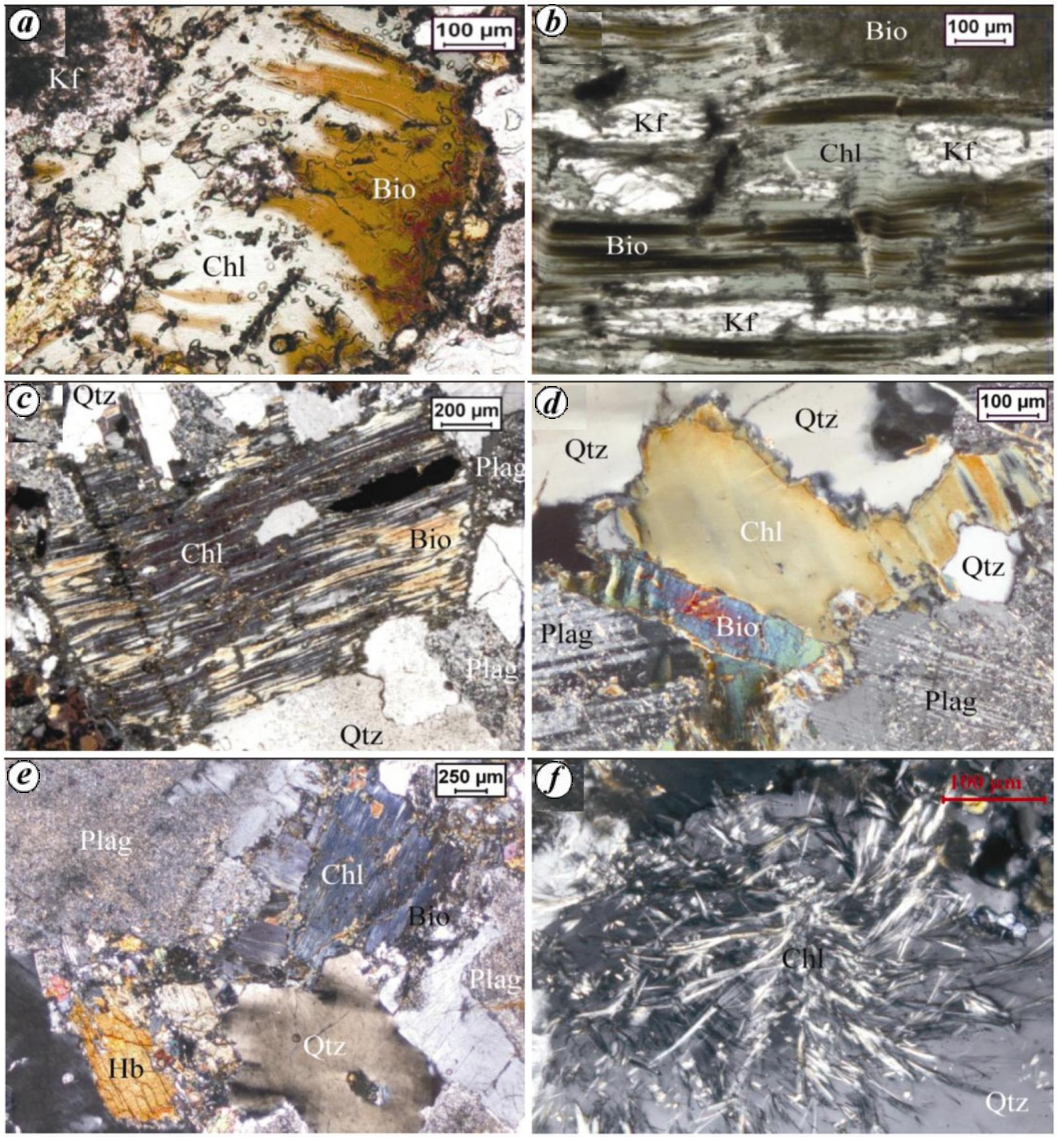

Figure 2. Chlorite mineral assemblage in MG under cross-polarized light. ***a***, Partial chloritization of biotite; ***b***, Partial chloritization of biotite with K-feldspar present as inclusions; ***c***, Chlorite–biotite–quartz–plagioclase; ***d***, Massive grains of chlorite with biotite–plagioclase–quartz; ***e***, Partial chloritization of hornblende and biotite; ***f***, Fibrous aggregates of chlorite. Mineral abbreviations: Bio, Biotite; Chl, Chlorite; Hb, Hornblende; Kf, Potash feldspar (sanidine); Plag, Plagioclase: Qtz, Quartz.

chlorite in the host granitoid due to the deuteric alteration by hydrothermal fluids. An attempt is made here to understand the physico-chemical conditions of hydrothermal alterations of silicate minerals in order to gain an insight into the late-stage hydrothermal fluid activities[5]. The chemistry of biotite, chlorite and epidote associated with the sulphide ore minerals indicates that these minerals play an important role in the aqueous solution at the time of mineralization. However, chlorite is the most dominant secondary phase in the host granitoid, whose role during the hydrothermal alteration is important and needs to be studied in detail.

In this study, thermodynamic modelling considering mineral fluid equilibria approach, is used to estimate the activities of various components of hydrothermal fluids which are possibly in kinetic equilibrium with the chlorite phase during deuteric alteration. Some of the important components of hydrothermal fluids are $a_{SiO_{2(aq)}}$ a_{Na^+}/a_{H^+}, a_{K^+}/a_{H^+}, $a_{Ca^{2+}}/a^2_{H^+}$, $a_{Mg^{2+}}/a^2_{H^+}$, $a_{Fe^{2+}}/a^2_{H^+}$, $a_{Fe^{3+}}/a^3_{H^+}$, and f_{O_2}. These components are compatible with chemical analyses of co-existing chlorite mineral assemblages as observed in the petrographic thin sections. These components are calculated and quantified for the Malanjkhand hydrothermal system to understand the chloritization phenomenon in the granitoid rocks.

Analytical methods

Polished petrographic thin sections were prepared for routine optical microscopy and EPMA analysis.

Table 1. Representative EPMA analyses of chlorites in wt% from the Malanjkhand Granitoid (MG) and Fe content reported as total FeO

Slide no.	01/2_12	01/2_12	01/2_12	01/2_12	01/2_12	01/2_12	01/2_12	01/2_12	01/2_12	05/2_12	05/2_12	05/2_12	05/2_12	05/2_12	05/2_12
Point #	2	8	9	11	12	13	14	15	16	17	22	24	25	26	27
SiO_2	23.73	26.80	28.82	25.96	31.64	25.57	27.01	26.08	28.59	29.41	27.90	27.00	28.28	26.73	28.61
TiO_2	0.06	0.05	0.08	0.51	1.22	0.32	0.08	0.14	0.19	0.04	0.02	0.11	0.08	0.05	0.01
Al_2O_3	19.62	19.86	18.72	18.68	16.64	17.58	18.83	20.45	18.47	19.38	18.58	19.88	18.44	18.32	18.65
FeO	31.15	31.49	26.92	30.18	25.87	28.91	31.36	30.10	30.30	21.19	20.73	21.37	20.08	20.73	20.83
MnO	0.38	0.27	0.29	0.19	0.20	0.16	0.20	0.27	0.28	0.16	0.22	0.21	0.23	0.20	0.23
MgO	12.85	12.40	13.43	12.24	10.31	12.07	12.50	12.81	13.41	19.59	20.98	20.43	21.41	20.70	19.65
CaO	0.07	0.10	0.15	0.10	0.05	0.10	0.18	0.09	0.12	0.01	0.01	0.23	0.08	0.02	0.04
Na_2O	0.00	0.03	0.13	0.05	0.02	0.00	0.05	0.00	0.01	0.00	0.00	0.01	0.05	0.00	0.00
K_2O	0.05	0.06	0.22	2.18	7.03	2.19	0.10	0.00	0.60	0.00	0.01	0.00	0.02	0.00	0.00
Total	87.91	91.06	88.76	90.09	92.98	86.90	90.31	89.94	91.97	89.78	88.45	89.24	88.67	86.75	88.02
Number of cations calculated on the basis of 14 oxygens															
Si	2.531	2.717	2.921	2.671	3.136	2.723	2.750	2.677	2.831	2.862	2.769	2.692	2.793	2.714	2.846
Ti	0.005	0.004	0.006	0.039	0.091	0.026	0.006	0.011	0.014	0.003	0.001	0.008	0.006	0.004	0.001
Al	2.466	2.373	2.236	2.265	1.944	2.206	2.260	2.474	2.155	2.223	2.173	2.336	2.146	2.193	2.187
Al^{iv}	1.464	1.279	1.073	1.290	0.773	1.251	1.244	1.312	1.155	1.135	1.229	1.299	1.201	1.282	1.153
Al^{vi}	1.002	1.094	1.164	0.975	1.171	0.955	1.016	1.162	1.000	1.088	0.944	1.037	0.945	0.911	1.034
Fe^{2+}	2.056	1.842	1.461	1.532	1.158	1.519	1.709	1.912	1.480	1.018	1.015	1.319	0.978	1.039	1.023
Fe^{3+}	0.722	0.828	0.822	1.065	0.987	1.056	0.961	0.672	1.029	0.707	0.706	0.463	0.680	0.722	0.711
Mn	0.034	0.023	0.025	0.017	0.017	0.014	0.017	0.023	0.023	0.013	0.018	0.018	0.019	0.017	0.019
Mg	2.043	1.874	2.029	1.877	1.523	1.916	1.897	1.960	1.979	2.842	3.104	3.037	3.152	3.134	2.914
Ca	0.008	0.011	0.016	0.011	0.005	0.011	0.020	0.010	0.013	0.001	0.001	0.025	0.008	0.002	0.004
Na	0.000	0.006	0.026	0.010	0.004	0.000	0.010	0.000	0.002	0.000	0.000	0.002	0.010	0.000	0.000
K	0.007	0.008	0.028	0.286	0.889	0.298	0.013	0.000	0.076	0.000	0.001	0.000	0.003	0.000	0.000
R^{2+}	4.134	3.740	3.515	3.426	2.698	3.450	3.624	3.896	3.483	3.873	4.138	4.374	4.149	4.190	3.956
Sum	5.873	5.686	5.571	5.773	5.754	5.769	5.644	5.739	5.602	5.670	5.790	5.900	5.795	5.825	5.704
X_{Mg}	0.498	0.504	0.581	0.551		0.526	0.526	0.506	0.736	0.736	0.754	0.697	0.763	0.751	0.740
X_{sud}	0.035	0.054	0.077	–		0.014	0.014	0.086	0.097	0.097	0.062	0.053	0.066	0.049	0.086
X_{clin}	0.052	0.033	0.049	–		0.008	0.008	0.067	0.112	0.112	0.120	0.218	0.140	0.110	0.114
X_{daph}	0.052	0.033	0.035	–		0.007	0.007	0.065	0.040	0.040	0.039	0.095	0.044	0.036	0.040
X_{MgAm}	0.064	0.024	0.008	–		0.005	0.005	0.052	0.029	0.029	0.051	0.112	0.049	0.059	0.033
X_{FeAm}	0.065	0.024	0.005	–		0.004	0.004	0.051	0.010	0.010	0.017	0.049	0.015	0.020	0.012
Sum	0.268	0.168	0.174	0.038		0.038	0.038	0.320	0.289	0.289	0.289	0.527	0.314	0.273	0.284

(*Contd*)

Table 1. (*Contd*)

Slide no.	05/2_12	05/2_12	05/2_12	05/2_12	05/2_12	05/2_12	05/2_12	05/2_12	78	03/18_12	284	56	56	56	714
Point #	28	29	30	32	34	35	38	40	62	92	118	108	123	124	149
SiO_2	28.15	25.02	25.47	26.87	32.13	29.45	30.69	32.26	26.69	27.32	27.61	24.88	29.05	26.11	27.73
TiO_2	0.05	0.03	0.07	0.06	0.12	0.02	0.07	0.03	0.11	0.12	0.00	0.04	0.43	0.00	0.04
Al_2O_3	19.40	19.64	20.78	20.51	18.02	19.53	17.99	17.63	20.00	19.99	15.92	18.97	16.58	19.65	17.93
FeO	21.11	20.66	20.42	20.83	20.67	21.49	20.40	19.44	31.37	24.36	24.44	29.46	26.38	27.17	22.90
MnO	0.19	0.22	0.19	0.14	0.26	0.21	0.19	0.16	0.38	0.35	0.34	0.16	0.29	0.23	0.35
MgO	20.84	20.07	20.11	20.69	20.79	19.85	21.49	21.22	12.16	17.05	17.00	10.89	11.84	13.50	17.07
CaO	0.05	0.08	0.06	0.01	0.01	0.00	0.06	0.08	0.05	0.02	0.16	0.21	0.31	0.01	0.06
Na_2O	0.00	0.02	0.07	0.01	0.01	0.01	0.01	0.00	0.02	0.08	0.06	0.09	0.08	0.00	0.04
K_2O	0.00	0.00	0.00	0.00	0.28	0.03	0.02	0.04	0.02	0.12	0.04	0.07	1.39	0.05	0.79
Total	89.79	85.74	87.17	89.12	92.29	90.59	90.92	90.86	90.80	89.41	85.57	84.77	86.35	86.72	86.91
Number of cations calculated on the basis of 14 oxygens															
Si	2.752	2.587	2.588	2.664	3.019	2.845	2.940	3.060	2.713	2.720	2.887	2.710	3.026	2.725	2.841
Ti	0.004	0.002	0.005	0.004	0.008	0.001	0.005	0.002	0.008	0.009	0.000	0.003	0.034	0.000	0.003
Al	2.235	2.393	2.489	2.397	1.996	2.224	2.031	1.971	2.396	2.346	1.962	2.435	2.036	2.417	2.165
Al^{iv}	1.245	1.411	1.407	1.331	0.972	1.153	1.055	0.938	1.279	1.271	1.113	1.287	0.940	1.275	1.156
Al^{vi}	0.990	0.982	1.082	1.066	1.024	1.070	0.977	1.032	1.117	1.075	0.849	1.148	1.096	1.142	1.009
Fe^{2+}	1.018	1.143	1.197	1.192	0.877	1.024	0.964	0.833	1.840	1.197	1.261	1.852	1.241	1.518	1.158
Fe^{3+}	0.708	0.643	0.538	0.536	0.747	0.712	0.670	0.709	0.827	0.832	0.876	0.832	1.057	0.854	0.805
Mn	0.016	0.019	0.016	0.012	0.021	0.017	0.015	0.013	0.033	0.030	0.030	0.015	0.026	0.020	0.030
Mg	3.037	3.093	3.046	3.058	2.913	2.859	3.069	3.000	1.842	2.531	2.650	1.768	1.839	2.101	2.607
Ca	0.005	0.009	0.007	0.001	0.001	0.000	0.006	0.008	0.005	0.002	0.018	0.025	0.035	0.001	0.007
Na	0.000	0.004	0.014	0.002	0.002	0.002	0.002	0.000	0.004	0.015	0.012	0.019	0.016	0.000	0.008
K	0.000	0.000	0.000	0.000	0.034	0.004	0.002	0.005	0.003	0.015	0.005	0.010	0.185	0.007	0.103
R^{2+}	4.071	4.256	4.260	4.262	3.811	3.901	4.049	3.846	3.715	3.757	3.941	3.635	3.106	3.639	3.795
Sum	5.774	5.895	5.900	5.866	5.618	5.688	5.706	5.601	5.671	5.697	5.702	5.668	5.494	5.643	5.727
X_{Mg}	0.749	0.730	0.718	0.720	–	0.736	0.761	–	0.500	0.679	0.678	0.488	–	0.581	0.692
X_{sud}	0.066	0.038	0.046	0.062	–	0.090	0.097	–	0.057	0.051	0.037	0.056	–	0.052	0.053
X_{clin}	0.112	0.121	0.158	0.175	–	0.110	0.160	–	0.031	0.045	0.047	0.030	–	0.029	0.073
X_{daph}	0.038	0.045	0.062	0.068	–	0.039	0.050	–	0.031	0.021	0.022	0.031	–	0.021	0.032
X_{MgAm}	0.054	0.107	0.135	0.111	–	0.033	0.014	–	0.024	0.031	0.009	0.024	–	0.023	0.021
X_{FeAm}	0.018	0.040	0.053	0.043	–	0.012	0.004	–	0.024	0.015	0.004	0.025	–	0.017	0.009
Sum	0.288	0.350	0.454	0.459	–	0.283	0.325	–	0.168	0.163	0.120	0.166	–	0.143	0.190

(*Contd*)

Table 1. (*Contd*)

Slide no.	714	714	714	714	09/496	09/496	319	319	319	019/472	019/472	024/15/12	106	106	106	106
Point #	150	151	152	153	9	10	81	82	83	103	105	115	84	85	86	87
SiO_2	26.90	27.33	27.97	27.09	28.38	29.05	25.60	25.32	25.88	25.15	25.54	27.33	28.69	28.31	28.63	26.57
TiO_2	0.00	0.07	0.11	0.02	0.01	0.00	0.00	0.07	0.00	0.00	0.00	0.05	0.02	0.00	0.01	0.06
Al_2O_3	18.05	17.43	17.15	16.84	16.82	14.90	20.01	20.10	19.84	19.70	18.48	16.92	18.90	18.55	19.11	18.84
FeO	23.07	23.38	22.19	22.72	21.14	19.30	24.47	23.16	24.18	28.94	27.59	23.37	23.61	22.73	23.12	22.63
MnO	0.37	0.37	0.34	0.40	0.44	0.27	0.32	0.31	0.43	0.27	0.26	0.34	0.00	0.00	0.00	0.00
MgO	17.37	17.79	17.02	17.70	19.16	20.09	16.06	16.40	16.27	12.43	13.45	16.32	17.50	16.98	17.67	17.83
CaO	0.05	0.01	0.05	0.02	0.14	0.12	0.04	0.02	0.01	0.02	0.01	0.03	0.02	0.02	0.02	0.02
Na_2O	0.02	0.04	0.07	0.00	0.02	0.03	0.00	0.02	0.00	0.02	0.00	0.01	0.05	0.02	0.02	0.00
K_2O	0.06	0.11	0.78	0.04	0.26	0.03	0.02	0.02	0.00	0.00	0.00	0.29	0.08	0.07	0.05	0.07
Total	85.89	86.53	85.68	84.83	86.37	83.79	86.52	85.42	86.61	86.53	85.33	84.66	88.85	86.68	88.62	86.03
Number of cations calculated on the basis of 14 oxygens																
Si	2.784	2.811	2.940	2.838	2.898	3.020	2.685	2.676	2.718	2.682	2.724	2.897	2.852	2.918	2.847	2.735
Ti	0.000	0.005	0.009	0.002	0.001	0.000	0.000	0.006	0.000	0.000	0.000	0.004	0.001	0.000	0.001	0.005
Al	2.202	2.113	2.124	2.079	2.024	1.826	2.474	2.504	2.456	2.476	2.323	2.114	2.215	2.254	2.240	2.286
Al^{iv}	1.216	1.183	1.052	1.161	1.101	0.980	1.315	1.318	1.282	1.318	1.276	1.099	1.146	1.082	1.152	1.260
Al^{vi}	0.985	0.930	1.072	0.918	0.924	0.846	1.159	1.186	1.174	1.158	1.047	1.015	1.068	1.172	1.088	1.026
Fe^{2+}	1.178	1.187	1.541	1.174	1.065	0.906	1.696	1.618	1.784	1.910	1.575	1.430	1.158	1.548	1.135	1.149
Fe^{3+}	0.819	0.825	0.410	0.816	0.740	0.772	0.451	0.430	0.340	0.671	0.886	0.642	0.805	0.412	0.788	0.799
Mn	0.032	0.032	0.030	0.035	0.038	0.024	0.028	0.028	0.038	0.024	0.023	0.031	0.000	0.000	0.000	0.000
Mg	2.680	2.728	2.667	2.764	2.917	3.114	2.512	2.584	2.547	1.976	2.139	2.579	2.594	2.609	2.620	2.737
Ca	0.006	0.001	0.006	0.002	0.015	0.013	0.004	0.002	0.001	0.002	0.001	0.003	0.002	0.002	0.002	0.002
Na	0.004	0.008	0.014	0.000	0.004	0.006	0.000	0.004	0.000	0.004	0.000	0.002	0.010	0.005	0.004	0.000
K	0.008	0.014	0.105	0.005	0.034	0.004	0.003	0.003	0.000	0.000	0.000	0.039	0.010	0.009	0.006	0.009
R^{2+}	3.890	3.947	4.238	3.974	4.020	4.044	4.236	4.230	4.370	3.911	3.737	4.039	3.752	4.157	3.755	3.886
Sum	5.712	5.725	5.844	5.716	5.737	5.686	5.853	5.854	5.884	5.746	5.671	5.741	5.646	5.757	5.643	5.722
X_{Mg}	0.695	0.697	0.634	0.702	0.732	0.335	0.597	0.615	0.588	0.508	0.576	0.643	0.691	0.628	0.698	0.704
X_{sud}	0.052	0.048	0.092	0.052	0.068	0.023	0.080	0.083	0.076	0.083	0.037	0.093	0.069	0.143	0.076	0.056
X_{clin}	0.058	0.062	0.285	0.067	0.114	0.004	0.167	0.178	0.219	0.068	0.024	0.141	0.067	0.249	0.073	0.066
X_{daph}	0.026	0.027	0.165	0.028	0.042	0.009	0.113	0.112	0.153	0.065	0.018	0.078	0.030	0.148	0.031	0.028
X_{MgAm}	0.027	0.022	0.019	0.021	0.019	0.003	0.103	0.112	0.109	0.053	0.018	0.023	0.020	0.030	0.022	0.037
X_{FeAm}	0.012	0.010	0.011	0.009	0.007	0.007	0.070	0.070	0.077	0.051	0.013	0.013	0.009	0.018	0.010	0.015
Sum	0.175	0.170	0.573	0.177	0.250	0.046	0.534	0.554	0.635	0.321	0.111	0.347	0.195	0.588	0.212	0.201

Table 2. Structural formulae of chlorite from MG and calculated temperature from chlorite compositions after Vidal *et al.*[14]

Slide no.	01/2_12	01/2_12	01/2_12	01/2_12	01/2_12	01/2_12	01/2_12	01/2_12	01/2_12	05/2_12	05/2_12	05/2_12	05/2_12	05/2_12	05/2_12
Point #	2	8	9	11	12	13	14	15	16	17	22	24	25	26	27
Fe/Fe + Mg	0.502	0.496	0.419	0.449	–	0.442	0.474	0.494	0.428	0.264	0.246	0.303	0.237	0.249	0.260
Al (M4)	0.278	0.172	0.178	–	–	–	0.039	0.328	–	0.293	0.294	0.537	0.320	0.278	0.289
v (M1)	0.127	0.314	0.429	0.227	–	0.231	0.356	0.261	0.398	0.330	0.210	0.100	0.205	0.175	0.296
Al M2–3	0.260	0.642	0.913	0.750	–	0.759	0.734	0.521	0.873	0.661	0.421	0.201	0.423	0.351	0.591
Al (M1)	0.464	0.279	0.073	0.290	–	0.251	0.244	0.312	0.155	0.135	0.229	0.299	0.201	0.282	0.153
(Fe + Mg) M1	0.375	0.383	0.473	0.467	–	0.503	0.384	0.404	0.423	0.522	0.543	0.583	0.574	0.526	0.532
(Fe + Mg) M2–3	3.725	3.333	3.017	2.943	–	2.932	3.223	3.469	3.036	3.338	3.577	3.773	3.556	3.647	3.405
Mg (M1)	0.187	0.193	0.275	0.257	–	0.281	0.202	0.204	0.242	0.384	0.409	0.407	0.438	0.395	0.394
Fe (M1)	0.188	0.190	0.198	0.210	–	0.223	0.182	0.199	0.181	0.138	0.134	0.177	0.136	0.131	0.138
Mg (M2–3)	1.856	1.681	1.754	1.620	–	1.635	1.696	1.756	1.737	2.458	2.695	2.630	2.714	2.739	2.520
Fe (M2–3)	1.868	1.652	1.263	1.322	–	1.297	1.528	1.713	1.299	0.880	0.882	1.142	0.843	0.908	0.884
(Fe + Mg + Al) A4	4.000	4.000	4.000	4.000	–	4.000	4.000	4.000	4.000	4.000	4.000	4.000	4.000	4.000	4.000
(Fe + Mg + Al + v) M1	1.000	1.000	1.000	1.000	–	1.000	1.000	1.000	1.000	1.000	1.000	1.000	1.000	1.000	1.000
Sum A4	4.000	4.000	4.000	4.000	–	4.000	4.000	4.000	4.000	4.000	4.000	4.000	4.000	4.000	4.000
X_{Si}	0.266	0.359	0.461	0.335	–	0.361	0.375	0.338	0.415	0.431	0.385	0.346	0.396	0.357	0.423
X_{al} (T)	0.732	0.640	0.536	0.645	–	0.626	0.622	0.656	0.578	0.567	0.615	0.650	0.601	0.641	0.577
Sum	0.998	0.998	0.997	0.980	–	0.987	0.997	0.995	0.993	0.999	0.999	0.996	0.997	0.998	1.000
X_{Mg}	0.187	0.193	0.275	0.257	–	0.281	0.202	0.204	0.242	0.384	0.409	0.407	0.438	0.395	0.394
X_{Fe}	0.188	0.190	0.198	0.210	–	0.223	0.182	0.199	0.181	0.138	0.134	0.177	0.136	0.131	0.138
X_{Al}	0.464	0.279	0.073	0.290	–	0.251	0.244	0.312	0.155	0.135	0.229	0.299	0.201	0.282	0.153
X_v	0.127	0.314	0.429	0.227	–	0.231	0.356	0.261	0.398	0.330	0.210	0.100	0.205	0.175	0.296
Sum	1.000	1.000	1.000	1.000	–	1.000	1.000	1.000	1.000	1.000	1.000	1.000	1.000	1.000	1.000
X_{Mg}	0.464	0.420	0.439	0.405	–	0.409	0.424	0.439	0.434	0.615	0.674	0.658	0.678	0.685	0.630
X_{Fe}	0.467	0.413	0.316	0.331	–	0.324	0.382	0.428	0.325	0.220	0.220	0.286	0.211	0.227	0.221
X_{Al}	0.065	0.161	0.228	0.188	–	0.190	0.184	0.130	0.218	0.165	0.105	0.050	0.106	0.088	0.148
Sum	1.000	1.000	1.000	1.000	–	1.000	1.000	1.000	1.000	1.000	1.000	1.000	1.000	1.000	1.000
X_{Al}	0.278	0.172	0.178	–	–	–	0.039	0.328	–	0.293	0.294	0.537	0.320	0.278	0.289
$X_{Fe^{3+}}$	0.722	0.828	0.822	1.065	–	1.056	0.961	0.672	1.029	0.707	0.706	0.463	0.680	0.722	0.711
Sum	1.000	1.000	1.000	–	–	–	1.000	1.000	–	1.000	1.000	1.000	1.000	1.000	1.000
$Fe^{3+}/(Fe^{3+} + Fe^{2+})$	0.260	0.310	0.360	0.410	–	0.460	0.360	0.260	0.100	0.410	0.410	0.260	0.410	0.410	0.410
X_{Mg}	0.498	0.504	0.581	0.548	–	0.597	0.526	0.506	0.588	0.736	0.754	0.697	0.763	0.751	0.740
T (°C)	535	260	215	115	–	110	257	273	165	251	331	450	323	380	269

(*Contd*)

Table 2. (*Contd*)

Slide no.	05/2_12	05/2_12	05/2_12	05/2_12	05/2_12	05/2_12	05/2_12	005/2_12	78	03/18_12	284	56	56	56	714
Point #	28	29	30	32	34	35	38	40	62	92	118	108	123	124	149
Fe/Fe + Mg	0.251	0.270	0.282	0.280	–	0.264	0.239	–	0.500	0.321	0.322	0.512	–	0.419	0.308
Al (M4)	0.292	0.357	0.462	0.464	–	0.288	0.330	–	0.173	0.168	0.124	0.168	–	0.146	0.195
v (M1)	0.226	0.105	0.100	0.134	–	0.312	0.294	–	0.329	0.303	0.298	0.332	–	0.357	0.273
Al M2–3	0.453	0.215	0.213	0.270	–	0.629	0.592	–	0.665	0.636	0.613	0.693	–	0.721	0.658
Al (M1)	0.245	0.411	0.407	0.331	–	0.153	0.055	–	0.279	0.271	0.113	0.287	–	0.275	0.156
(Fe + Mg) M1	0.513	0.465	0.477	0.523	–	0.518	0.636	–	0.359	0.397	0.559	0.366	–	0.348	0.540
(Fe + Mg) M2–3	3.542	3.772	3.766	3.727	–	3.366	3.398	–	3.323	3.331	3.352	3.254	–	3.271	3.224
Mg (M1)	0.384	0.339	0.343	0.376	–	0.381	0.484	–	0.180	0.270	0.379	0.179	–	0.202	0.374
Fe (M1)	0.129	0.125	0.135	0.147	–	0.137	0.152	–	0.180	0.127	0.180	0.187	–	0.146	0.166
Mg (M2–3)	2.652	2.754	2.704	2.682	–	2.478	2.585	–	1.663	2.261	2.271	1.589	–	1.899	2.233
Fe (M2–3)	0.889	1.018	1.063	1.045	–	0.888	0.812	–	1.660	1.069	1.081	1.664	–	1.372	0.992
(Fe + Mg + Al) A4	4.000	4.000	4.000	4.000	–	4.000	4.000	–	4.000	4.000	4.000	4.000	–	4.000	4.000
(Fe + Mg + Al + v) M1	1.000	1.000	1.000	1.000	–	1.000	1.000	–	1.000	1.000	1.000	1.000	–	1.000	1.000
Sum A4	4.000	4.000	4.000	4.000	–	4.000	4.000	–	4.000	4.000	4.000	4.000	–	4.000	4.000
X_{Si}	0.376	0.293	0.294	0.332	–	0.423	0.470	–	0.356	0.360	0.444	0.355	–	0.363	0.421
$X_{Al}(T)$	0.622	0.705	0.703	0.666	–	0.577	0.527	–	0.639	0.635	0.556	0.643	–	0.637	0.578
Sum	0.998	0.999	0.997	0.998	–	0.999	0.997	–	0.996	0.996	1.000	0.998	–	1.000	0.998
X_{Mg}	0.384	0.339	0.343	0.376	–	0.381	0.484	–	0.180	0.270	0.379	0.179	–	0.202	0.374
X_{Fe}	0.129	0.125	0.135	0.147	–	0.137	0.152	–	0.180	0.127	0.180	0.187	–	0.146	0.166
X_{Al}	0.245	0.411	0.407	0.331	–	0.153	0.055	–	0.279	0.271	0.113	0.287	–	0.275	0.156
X_v	0.226	0.105	0.100	0.134	–	0.312	0.294	–	0.329	0.303	0.298	0.332	–	0.357	0.273
Sum	1.000	1.000	1.000	1.000	–	1.000	1.000	–	1.000	1.000	1.000	1.000	–	1.000	1.000
X_{Mg}	0.663	0.689	0.676	0.670	–	0.619	0.646	–	0.416	0.565	0.568	0.397	–	0.475	0.558
X_{Fe}	0.222	0.255	0.266	0.261	–	0.222	0.203	–	0.415	0.267	0.270	0.416	–	0.343	0.248
X_{Al}	0.113	0.054	0.053	0.067	–	0.157	0.148	–	0.166	0.159	0.153	0.173	–	0.180	0.164
Sum	1.000	1.000	1.000	1.000	–	1.000	1.000	–	1.000	1.000	1.000	1.000	–	1.000	1.000
X_{Al}	0.292	0.357	0.462	0.464	–	0.288	0.330	–	0.173	0.168	0.124	0.168	–	0.146	0.195
$X_{Fe^{3+}}$	0.708	0.643	0.538	0.536	–	0.712	0.670	–	0.827	0.832	0.876	0.832	–	0.854	0.805
Sum	1.000	1.000	1.000	1.000	–	1.000	1.000	–	1.000	1.000	1.000	1.000	–	1.000	1.000
$Fe^{3+}/(Fe^{3+} + Fe^{2+})$	0.410	0.360	0.310	0.310	–	0.410	0.410	–	0.460	0.310	0.410	0.410	–	0.310	0.460
X_{Mg}	0.749	0.730	0.718	0.720	–	0.736	0.761	–		0.500	0.679	0.678	–	0.488	0.581
T (°C)	324	566	559	367	–	260	258	–	250	278	281	230	–	212	271

(*Contd*)

Table 2. (*Contd*)

Slide no.	714	714	714	714	09/496	09/496	319	319	319	019/472	019/472	024/15/12	106	106	106	106
Point #	150	151	152	153	9	10	81	82	83	103	105	115	84	85	86	87
Fe/Fe + Mg	0.305	0.303	0.366	0.298	0.268	0.665	0.403	0.385	0.412	0.492	0.424	0.357	0.309	0.372	0.302	0.296
Al (M4)	0.181	0.175	0.590	0.184	0.260	0.049	0.549	0.570	0.660	0.329	0.114	0.358	0.195	0.588	0.212	0.201
v (M1)	0.288	0.275	0.156	0.284	0.263	0.465	0.147	0.146	0.116	0.254	0.329	0.259	0.354	0.243	0.357	0.278
Al M2–3	0.588	0.572	0.430	0.574	0.563	1.001	0.296	0.298	0.231	0.511	0.657	0.559	0.727	0.501	0.724	0.565
Al (M1)	0.216	0.183	0.052	0.161	0.101	0.203	0.315	0.318	0.282	0.318	0.276	0.099	0.146	0.082	0.152	0.260
(Fe + Mg)M1	0.463	0.510	0.762	0.520	0.598	0.265	0.511	0.509	0.564	0.404	0.372	0.612	0.500	0.674	0.491	0.462
(Fe + Mg) M2–3	3.395	3.405	3.445	3.419	3.384	2.918	3.697	3.693	3.767	3.482	3.342	3.397	3.252	3.483	3.264	3.424
Mg (M1)	0.322	0.355	0.483	0.365	0.438	0.089	0.305	0.313	0.332	0.205	0.214	0.394	0.346	0.423	0.343	0.325
Fe (M1)	0.142	0.155	0.279	0.155	0.160	0.176	0.206	0.196	0.232	0.199	0.158	0.218	0.154	0.251	0.148	0.137
Mg (M2–3)	2.358	2.373	2.183	2.399	2.479	0.978	2.207	2.271	2.216	1.771	1.924	2.185	2.248	2.186	2.278	2.411
Fe (M2–3)	1.037	1.032	1.262	1.019	0.905	1.941	1.490	1.422	1.552	1.712	1.417	1.211	1.004	1.297	0.986	1.013
(Fe + Mg + Al) A 4	4.000	4.000	4.000	4.000	4.000	4.000	4.000	4.000	4.000	4.000	4.000	4.000	4.000	4.000	4.000	4.000
(Fe + Mg + Al + v) M1	1.000	1.000	1.000	1.000	1.000	1.000	1.000	1.000	1.000	1.000	1.000	1.000	1.000	1.000	1.000	1.000
Sum A4	4.000	4.000	4.000	4.000	4.000	4.000	4.000	4.000	4.000	4.000	4.000	4.000	4.000	4.000	4.000	4.000
X_{Si}	0.392	0.406	0.470	0.419	0.449	0.396	0.343	0.338	0.359	0.341	0.362	0.449	0.426	0.459	0.424	0.367
X_{Al}(T)	0.608	0.592	0.526	0.580	0.550	0.601	0.657	0.659	0.641	0.659	0.638	0.549	0.573	0.541	0.576	0.630
Sum	1.000	0.997	0.996	0.999	1.000	0.998	1.000	0.997	1.000	1.000	1.000	0.998	0.999	1.000	1.000	0.998
X_{Mg}	0.322	0.355	0.483	0.365	0.438	0.089	0.305	0.313	0.332	0.205	0.214	0.394	0.346	0.423	0.343	0.325
X_{Fe}	0.142	0.155	0.279	0.155	0.160	0.176	0.206	0.196	0.232	0.199	0.158	0.218	0.154	0.251	0.148	0.137
X_{Al}	0.216	0.183	0.052	0.161	0.101	0.203	0.315	0.318	0.282	0.318	0.276	0.099	0.146	0.082	0.152	0.260
X_{v}	0.288	0.275	0.156	0.284	0.263	0.465	0.147	0.146	0.116	0.254	0.329	0.259	0.354	0.243	0.357	0.278
Sum	1.000	1.000	1.000	1.000	1.000	1.000	1.000	1.000	1.000	1.000	1.000	1.000	1.000	1.000	1.000	1.000
X_{Mg}	0.589	0.593	0.546	0.600	0.620	0.244	0.552	0.568	0.554	0.443	0.481	0.546	0.562	0.546	0.569	0.603
X_{Fe}	0.259	0.258	0.315	0.255	0.226	0.485	0.373	0.355	0.388	0.428	0.354	0.303	0.251	0.324	0.247	0.253
X_{Al}	0.147	0.143	0.108	0.143	0.141	0.250	0.074	0.074	0.058	0.128	0.164	0.140	0.182	0.125	0.181	0.141
Sum	1.000	1.000	1.000	1.000	1.000	1.000	1.000	1.000	1.000	1.000	1.000	1.000	1.000	1.000	1.000	1.000
X_{Al}	0.181	0.175	0.590	0.184	0.260	0.049	0.549	0.570	0.660	0.329	0.114	0.358	0.195	0.588	0.212	0.201
$X_{Fe^{3+}}$	0.819	0.825	0.410	0.816	0.740	0.951	0.451	0.430	0.340	0.671	0.886	0.642	0.805	0.412	0.788	0.799
Sum	1.000	1.000	1.000	1.000	1.000	1.000	1.000	1.000	1.000	1.000	1.000	1.000	1.000	1.000	1.000	1.000
$Fe^{3+}/(Fe^{3+} + Fe^{2+})$	0.410	0.410	0.410	0.210	0.410		0.410	0.210	0.210	0.160	0.260	0.360	0.310	0.410	0.210	0.410
X_{Mg}	0.692	0.695	0.697	0.634	0.702		0.732	0.597	0.615	0.588	0.508	0.576	0.643	0.691	0.628	0.698
T (°C)	290	288	261	284	284		395	377	416	276	242	277	239	265	239	300

Chloritization of biotite and hornblende assemblages is mainly selected for electron microprobe analysis. Chlorite phases are identified in polished thin sections of granitoid samples and analysed with five WDS spectrometers attached with CAMECA SX100 Electron Microprobe at EPMA Laboratory, Geological Survey of India, Kolkata. Experimental conditions of 20 keV accelerating voltage, 15 nA beam current, 1 μm beam size and 20 sec counting time were applied for major element analysis. All natural silicate standards have been used for routine calibrations. Chlorite chemical compositions obtained by EPMA (Table 1) were processed using the program for chlorite solid solution model developed by Vidal *et al.*[14]. Estimated mineralogical formula, crystal structural parameters and temperature of chlorite formation are presented in Tables 1 and 2.

Chlorite composition

In the MG, chlorite comprises of SiO_2 content 23.73–32.26 wt%, Al_2O_3 14.90–20.78 wt%, FeO_{tot} 19.30–31.49 wt%, MgO 10.31–1.49 wt% and other constituents such as TiO_2, MnO, CaO and Na_2O are in trace quantity (<1 wt%). However, in some cases observed K_2O is very high because chlorite and biotite occur together in most of the cases (Figure 2 *a–d*). Photomicrographs also indicate that most of the chlorites are the product of hydrothermal alteration of primary biotite. Chemical composition of chlorites from MG is plotted in FeO–MgO–Al_2O_3 triangular diagram (Figure 3 *a*) in the system FMASH using the classification scheme of Fleming and Fawcett[15]. The chlorites fall in daphnite–pseudothuringite field of Chernosky *et al.*[16]. Crystallochemical classification of chlorite on the unified projection system[2] inferred that these are mostly di-trioctahedral (DT) phyllosilicates (Figure 3 *b*). Natural chlorite shows three kinds of substitution mechanisms. Fe–Mg_{-1} (FM) substitution extends over the whole range between Mg and Fe end-members, Tschermak (TK) substitution is restricted to chlorite compositions between clinochlore–daphnite and DT substitution corresponds to the coupled exchange of Mg and Fe for Al (ref. 14). Chlorites from MG show affinity for DT substitution which is more prominent than TK substitution (Figure 3 *c*). Chlorite solid solution model of Vidal *et al.*[14] is used to estimate the temperature of formation and a range from 110°C to 400°C was obtained with variable mole fraction of end-member components (Figure 3 *d*). However, high temperature (>400°C) is also obtained in some chlorite compositions from MG possibly due to uncertainty proposed by Vidal *et al.*[14] in the thermodynamic modelling of chlorite solid solution. A chlorite classification scheme was also proposed by Hey[17], which is used to discriminate oxidized and unoxidized types. Chlorites from MG, mostly belong to pyrochlorite–rapidolite field in the Si versus $Fe^{2+} + Fe^{3+}$ diagram (Figure 3 *e*). Oxidized chlorite with Si content between 5.6 and 6.2 atoms per formula unit (apfu) is mostly pyrochlorite[2]. However, unoxidized chlorites are common in MG with Si content less than 5.6 apfu. These chlorites are not restricted to hydrothermal mineralization zone which is related to low oxidation conditions in MG[5]. Further, rise in oxygen fugacity favour chloritization in MG. The chlorite composition in Si versus Fe/(Fe + Mg +Mn) diagram indicates three different states of Fe/(Fe + Mg + Mn) ratios with variable content of Si which may be due to the fact that Fe–Mg substitution is not affected by the Si content in chlorite (Figure 3 *f*).

Chlorite solid solution

The four-component chlorite solid solution model proposed by Vidal *et al.*[14] has been adopted in the present study for the estimation of temperature, mole fractions and activities of its four end-member components. Activities of end-member components are calculated from chlorite compositions and are presented in Table 3. Phase relation for chlorite solid solution model is consistent with the activities of their end-member components. There is variation in activities of end-members up to –5 logarithm units, in accordance with the change in the temperature of the hydrothermal fluids (Figure 4 *a–d*). Compositions of co-existing calcic-, sodic- and potassic-feldspars in the temperature range 150–600°C were considered and the activity composition relations used for these components were according to assumed Raoult's law. At temperature ≤ 320°C, activity of feldspar end-members and quartz is assumed as unity[18]. Compositional analyses of tremolite solid solutions reveal that $\log(a_{Ca_2Mg_5Si_8O_{22}(OH)_2})$ ranges from – 3.155 to –1.208, considered from an earlier study (D. Pandit, unpublished). Raoult's law approximations are used in activity composition relations of the $Ca_2Mg_5Si_8O_{22}(OH)_2$ component because of uncertainties in measurements of mineral compositions and crystallographic site distribution of cations in tremolite solid solution[19]. According to theoretical consideration of Bird and Norton[18] for thermodynamic modelling of mineral fluid equilibria in the temperature range 150–600°C, fluid phases maintains kinetic equilibrium with α-quartz in the Malanjkhand hydrothermal system during chloritization.

Mineral fluid equilibria

Hydrothermal processes in any rock will alter its mineralogical and sometimes chemical composition. The physicochemical conditions of its environment are changed in such a way that the rock is no longer in kinetic equilibrium with its environment. Changes in temperature or pressure cause alteration of the rock, with the formation of new minerals that are in equilibrium with the new

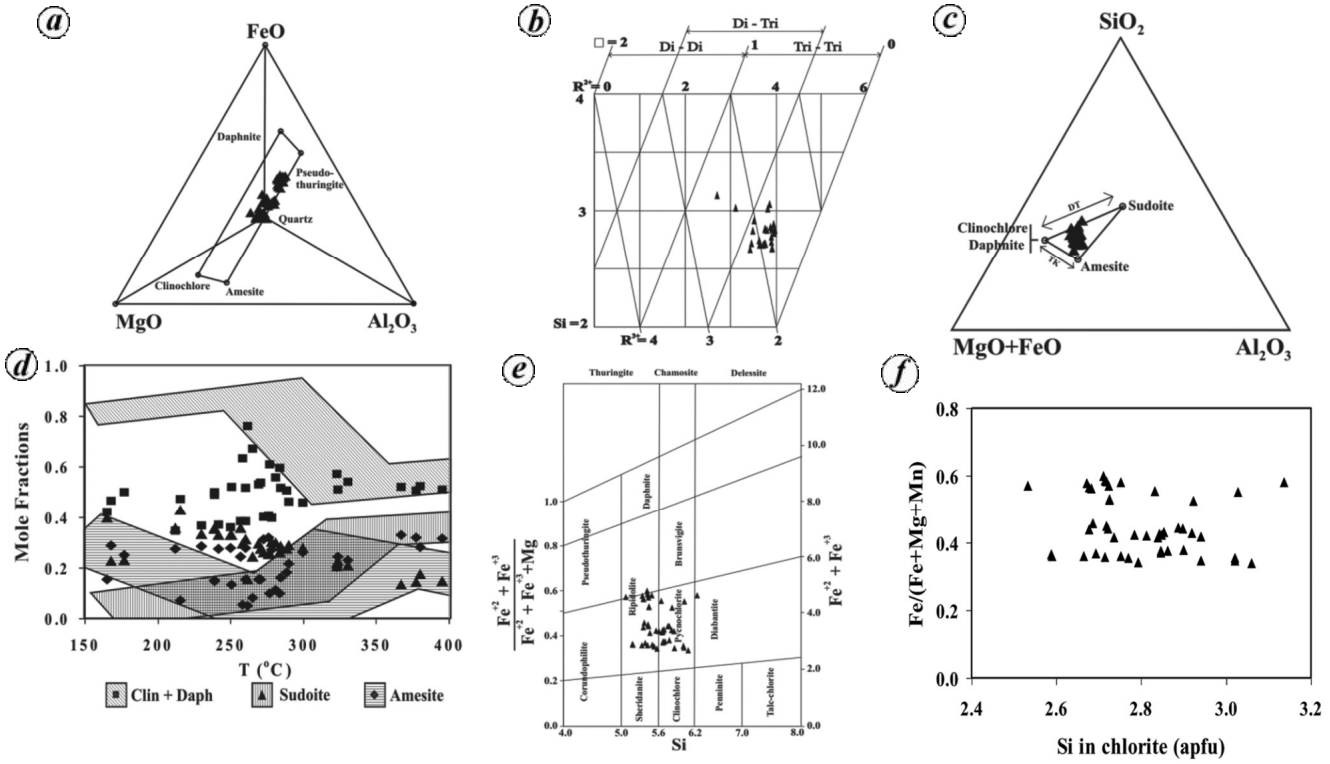

Figure 3. Mineral composition of chlorites of MG: ***a***, FeO–MgO–Al_2O_3 triangular diagram for end-members of chlorite[15,16]; ***b***, R^{3+}–R^{2+} binary diagram for di–tri octahedral classes of chlorites[2]; ***c***, SiO_2–(MgO + FeO)–Al_2O_3 ternary diagram of chlorite end-members and substitution considered in chlorite solid solution model[14]; ***d***, Calculated mole fraction of clinochlore + daphnite (square), sudoite (triangle), and amesite (diamond) in chlorites at fixed $X_{Mg} = 0.5$ equilibrated with quartz and H_2O (ref. 14); ***e***, Chlorite classification[2,17]; ***f***, Variation diagram of Si versus Fe/(Fe + Mg + Mn) for chlorite.

physico-chemical conditions. Generally, entry of an external hydrothermal fluid brings changes in the chemistry of the environment which interrupted the kinetic equilibrium with the rock. It may cause large changes both in the chemistry and the mineralogy of the host rock, especially if the physico-chemical environment changes are combined with an increase in temperature. The ultimate result of the alteration process will be that the rock has adapted to the new situation and is in equilibrium with the new physico-chemical environment. Application of mineral fluid equilibria modelling to hydrothermal alteration faces two main problems, i.e. the geometry of fluid–rock interaction and quality of thermodynamic database used, even for the limiting assumption of local equilibration between fluids and minerals[20]. However, theoretical geochemistry allows quantitative interpretation of the chemical characteristics of hydrothermal solution and compositional relations among aqueous solutions, gases and minerals at high pressures and temperatures from the equations and high level of internal consistency of multicomponent thermodynamic database given by several workers[21–32]. The present approach is based on the relative importance of chloritization processes likely to affect the composition of hydrothermal alteration assemblages is necessarily based on the assumption that equilibrium is attained among at least some of the fluid and mineral components. According to Bird and Norton[18], equilibrium condition among mineral components and an aqueous solution can be written as

$$0 = \sum_{l}^{i} n_{l,r}\psi_l + \sum_{l}^{i} n_{l,r}\phi_l, \tag{1}$$

where the subscripts i and l respectively denote the mineral components (ψ) and the species in the coexisting fluid (ϕ). In eq. (1), n is the stoichiometric coefficient of the reaction, which is assumed as positive for products and negative for reactants. The logarithm of the law of mass action equation for reaction (1) allows the thermodynamic activities of aqueous species to be written as

$$\sum_{l}^{i} n_{l,r} \log\left(\frac{a_{\phi_l}}{a_{H^+}^{z}}\right) = \log K_{P,T,r} - \sum_{l}^{i} n_{l,r} \log a_{\psi_l}, \tag{2}$$

$K_{P,T,r}$ (2) is the equilibrium constant for the rth statement of reaction (1) at the subscripted pressure (P) and temperature (T). It is estimated that for any balanced geochemical reaction involving j phase component[14], the equilibrium condition is

$$0 = \sum_{j} v_j \Delta G_j^{P,T} - RT \ln K_{P,T,r}, \tag{3}$$

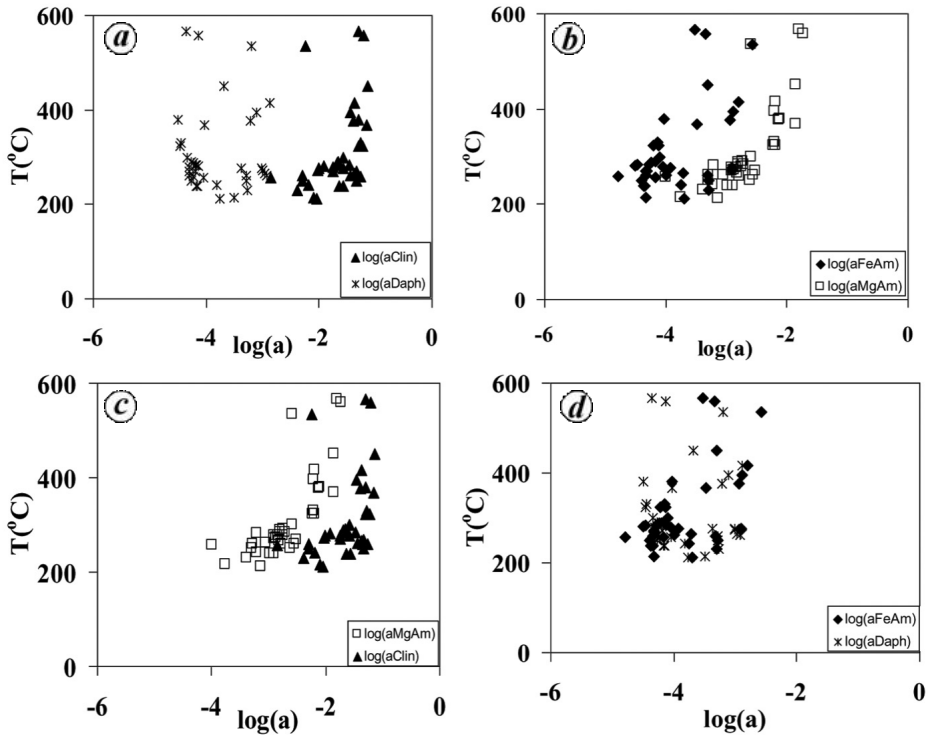

Figure 4. Temperature dependence of activities of end-member components according to the chlorite solid solution model[14]. Comparison of activities of four end-member components of chlorites in MG: ***a***, Clinochlore (Clin) with daphnite (Daph); ***b***, Fe-amesite (FeAm) with Mg-amesite; ***c***, Mg-amesite with clinochlore; ***d***, Fe-amesite with daphnite.

where $\Delta G_j^{P,T}$ is the apparent Gibbs free energy of formation obtained from SUPRT92 database[33]; a the activity of the subscripted reaction component and z is the change of the lth aqueous species. Gradient in the activity of the lth aqueous species in geothermal systems is represented by

$$\frac{\mathrm{d}}{\mathrm{d}Z}\log\left(\frac{a_{\phi_l}}{a_{\mathrm{H}^+}^z}\right)=\left[\frac{\partial}{\partial T}\log\left(\frac{a_{\phi_l}}{a_{\mathrm{H}^+}^z}\right)_{P,\phi}\frac{\mathrm{d}T}{\mathrm{d}Z}\right]$$

$$+\left[\frac{\partial}{\partial P}\log\left(\frac{a_{\phi_l}}{a_{\mathrm{H}^+}^z}\right)_{T,\phi}\frac{\mathrm{d}P}{\mathrm{d}Z}\right], \qquad (4)$$

where ϕ denotes activity constant of all aqueous species other than the lth and Z is either a unit distance along a fluid path or depth down a drill hole. Writing the total differential represented by eq. (4) in terms of eq. (2) gives

$$\sum_l^i n_{l,r}\frac{\mathrm{d}}{\mathrm{d}Z}\log\left(\frac{a_{\phi_l}}{a_{\mathrm{H}^+}^z}\right)$$

$$=\frac{\Delta H^0_{P,T,r}}{2.303RT^2}\frac{\mathrm{d}T}{\mathrm{d}Z}-\frac{\Delta V^0_{P,T,r}}{2.303RT}\frac{\mathrm{d}P}{\mathrm{d}Z}$$

$$-\sum_l^i n_{i,r}\left[\left(\frac{\partial}{\partial T}\log a_{\phi_l}\right)_{P,\psi,\phi_l}\frac{\mathrm{d}T}{\mathrm{d}Z}+\left(\frac{\partial}{\partial T}\log a_{\phi_l}\right)_{T,\psi,\phi_l}\frac{\mathrm{d}P}{\mathrm{d}Z}\right], \qquad (5)$$

where $\Delta H^0_{P,T,r}$ and $\Delta V^0_{P,T,r}$ are the standard modal enthalpy and volume respectively for the rth statement of reaction (1) and ψ refers to activity constants of all mineral components, excluding the ith.

Chloritization in the Malanjkhand Granitoid

Hydrothermal mineralization in the Paleoproterozoic MG provides an excellent site to study the chloritization phenomenon in the granite ore system. Photomicrographs suggest that chlorite and its associated mineral assemblages occurred in micro-domain. Other mineral phases in this micro-domain are K-feldspar, plagioclase and quartz in addition to the primary biotite and hornblende. These assemblages of albite, K-feldspar/sanidine, plagioclase/anorthite and aqueous solution are represented by the following kinetic equilibrium reactions

$$\mathrm{Chl_{Mg}}+3\mathrm{SiO_{2(aq)}}+8\mathrm{H^+}+2\mathrm{K^+}$$

$$=2\mathrm{Kf}+8\mathrm{H_2O}+5\mathrm{Mg^{2+}}, \qquad (6)$$

Table 3. Calculated activities of end-member components of chlorite solid solution[14] from mineral composition data given in Table 1

Slide no.	Point #	$\log(a_{Clin})$	$\log(a_{Daph})$	$\log(a_{Sud})$	$\log(a_{MgAm})$	$\log(a_{FeAm})$
01/2_12	2	–2.2	–3.2	–2.3	–2.6	–2.6
01/2_12	8	–2.3	–3.3	–1.7	–3.3	–3.3
01/2_12	9	–2.1	–3.5	–1.4	–3.8	–4.3
01/2_12	11	–	–	–	–	–
01/2_12	12	–	–	–	–	–
01/2_12	13	–	–	–	–	–
01/2_12	14	–2.9	–4.0	–2.2	–4.0	–4.2
01/2_12	15	–2.0	–3.0	–1.5	–2.9	–2.9
01/2_12	16	–	–	–	–	–
05/2_12	17	–1.3	–4.3	–1.0	–2.6	–4.4
05/2_12	22	–1.3	–4.4	–1.3	–2.2	–4.1
05/2_12	24	–1.1	–3.7	–1.7	–1.9	–3.3
05/2_12	25	–1.2	–4.5	–1.2	–2.2	–4.2
05/2_12	26	–1.3	–4.5	–1.4	–2.1	–4.0
05/2_12	27	–1.3	–4.3	–1.1	–2.5	–4.3
05/2_12	28	–1.3	–4.5	–1.2	–2.2	–4.1
05/2_12	29	–1.3	–4.4	–1.9	–1.8	–3.5
05/2_12	30	–1.2	–4.1	–1.8	–1.7	–3.3
05/2_12	32	–1.2	–4.0	–1.5	–1.8	–3.5
05/2_12	34	–	–	–	–	–
05/2_12	35	–1.3	–4.3	–1.1	–2.6	–4.3
05/2_12	38	–1.3	–4.2	–1.0	–2.8	–4.8
05/2_12	40	–	–	–	–	–
78	62	–2.3	–3.3	–1.7	–3.3	–3.3
03/18_12	92	–1.8	–4.3	–1.4	–2.7	–4.0
284	118	–1.9	–4.1	–1.6	–3.2	–4.5
56	108	–2.4	–3.3	–1.7	–3.4	–3.3
56	123	–	–	–	–	–
56	124	–2.0	–3.8	–1.5	–3.1	–3.7
714	149	–1.8	–4.2	–1.3	–2.9	–4.3
714	150	–1.7	–4.3	–1.4	–2.7	–4.2
714	151	–1.7	–4.2	–1.4	–2.8	–4.2
714	152	–1.4	–2.9	–1.2	–3.0	–4.0
714	153	–1.6	–4.2	–1.4	–2.8	–4.3
09/496	9	–1.5	–4.2	–1.2	–2.7	–4.5
09/496	10	–	–	–	–	–
319	81	–1.5	–3.1	–1.5	–2.2	–2.9
319	82	–1.4	–3.2	–1.5	–2.1	–2.9
319	83	–1.4	–2.9	–1.7	–2.2	–2.8
019/472	103	–2.0	–3.0	–1.5	–2.8	–2.9
019/472	105	–2.2	–3.8	–1.7	–3.2	–3.7
024/15/12	115	–1.6	–3.4	–1.2	–2.9	–3.9
106	84	–1.6	–4.2	–1.2	–3.0	–4.4
106	85	–1.4	–3.0	–1.0	–2.8	–3.7
106	86	–1.6	–4.2	–1.2	–2.9	–4.3
106	87	–1.6	–4.3	–1.3	–2.6	–4.1
	Min	–2.9	–4.5	–2.3	–4.0	–4.8
	Max	–1.1	–2.9	–1.0	–1.7	–2.6

$$Chl_{Mg} + 3SiO_{2(aq)} + 8H^+ + 2Na^+ = 2Ab + 8H_2O + 5Mg^{2+}, \quad (7)$$

$$Chl_{Fe} + 3SiO_{2(aq)} + 8H^+ + 2Na^+ = 2Ab + 8H_2O + 5Fe^{2+}, \quad (8)$$

$$Tr + An + 6H^+ = Chl_{Mg} + 7SiO_{2(aq)} + 3Ca^{2+}, \quad (9)$$

$$Tr + An + 3H_2O = Chl_{Mg} + 3CaSiO_3 + 4SiO_{2(aq)}, \quad (10)$$

$$Chl_{Mg} + 10H^+ = Kln + SiO_{2(aq)} + 7H_2O + 5Mg^{2+}, \quad (11)$$

The equilibrium reaction constant for all the above reactions is derived from the SUPRT92 thermodynamic database of Johanson *et al.*[33] in the temperature range 50–600°C at $P = 1$ kbar. Third-degree polynomial regression is applied to obtain the best approximation and these are expressed as follows

$$\log K_6 = -3 \times 10^{-7} T^3 + 0.0006T^2 - 0.3825T + 122.99, \quad (12)$$

Table 4. Calculated activities of aqueous species in hydrothermal fluid calculated from chlorite compositions

Slide no.	Point #	T (°C)	$\log(a_{Fe^{3+}})$	$\log(a_{SO_{2(aq)}})$	$\log\left(\frac{a_{Ca^{2+}}}{(a_{H^+})^2}\right)$	$\log\left(\frac{a_{Mg^{2+}}}{(a_{H^+})^2}\right)$	$\log\left(\frac{a_{Fe^{2+}}}{(a_{H^+})^2}\right)$	$\log\left(\frac{a_{Na^{2+}}}{a_{H^+}}\right)$	$\log\left(\frac{a_{K^+}}{a_{H^+}}\right)$
01/2_12	2	535	–1.820	–2.226	5.554	3.122	–1.109	4.808	–9.813
01/2_12	8	260	–1.618	–2.952	7.378	5.168	1.540	6.108	–10.917
01/2_12	9	215	–1.439	–3.229	7.974	6.149	2.299	6.639	–11.485
01/2_12	11	168	–1.672	–4.537	9.670	8.361	4.992	9.229	–10.414
01/2_12	12	177	–1.636	–4.489	9.543	8.126	4.800	9.138	–10.181
01/2_12	13	257	–1.453	–2.828	7.274	5.086	1.292	5.859	–11.229
01/2_12	14	273	–1.716	–2.961	7.305	5.002	1.433	6.134	–10.630
01/2_12	15	165	–1.335	–4.645	9.805	8.532	5.130	9.442	–10.311
01/2_12	16	251	–0.960	–3.233	7.720	5.578	1.305	6.667	–10.553
05/2_12	17	331	–0.894	–2.922	6.942	4.330	–0.001	6.087	–9.775
05/2_12	22	290	–1.238	–2.867	7.109	4.698	0.807	5.955	–10.503
05/2_12	24	450	–1.205	–2.615	6.165	3.425	–1.190	5.540	–9.412
05/2_12	25	323	–0.903	–2.942	7.004	4.424	0.086	6.124	–9.839
05/2_12	26	380	–0.889	–2.754	6.553	3.807	–0.521	5.779	–9.593
05/2_12	27	269	–0.946	–3.162	7.531	5.256	0.919	6.534	–10.308
05/2_12	28	324	–0.910	–2.941	6.997	4.413	0.129	6.121	–9.830
05/2_12	29	566	–1.041	–2.443	5.706	3.464	–1.564	5.258	–9.223
05/2_12	30	559	–1.150	–2.464	5.741	3.453	–1.506	5.297	–9.218
05/2_12	32	367	–1.102	–2.787	6.641	3.920	–0.377	5.839	–9.643
05/2_12	34	260	–0.957	–3.210	7.636	5.426	1.164	6.624	–10.401
05/2_12	35	258	–0.960	–2.960	7.400	5.204	1.579	6.124	–10.944
05/2_12	38	250	–1.626	–3.136	7.629	5.496	1.312	6.472	–10.770
05/2_12	40	301	–0.930	–2.987	7.166	4.693	0.464	6.202	–10.077
78	62	307	–0.988	–2.886	7.032	4.528	0.379	6.003	–10.185
03/18_12	92	283	–0.949	–3.039	7.322	4.954	0.779	6.295	–10.284
56	108	281	–1.072	–2.952	7.248	4.892	0.854	6.121	–10.494
56	123	230	–1.691	–3.078	7.711	5.746	2.093	6.344	–11.378
56	124	212	–1.282	–3.259	8.027	6.232	2.252	6.697	–11.512
714	149	271	–1.139	–3.038	7.395	5.105	0.994	6.287	–10.516
714	150	290	–1.004	–2.980	7.222	4.812	0.660	6.182	–10.275
714	151	288	–1.014	–2.982	7.236	4.837	0.704	6.184	–10.308
714	152	261	–1.600	–3.162	7.582	5.364	1.670	6.529	–10.475
714	153	284	–0.993	–3.010	7.287	4.913	0.780	6.238	–10.323
09/496	9	284	–1.014	–3.053	7.330	4.956	0.786	6.324	–10.237
09/496	10	395	–1.537	–2.685	6.424	3.660	–0.193	5.649	–9.610
319	81	377	–1.507	–2.750	6.561	3.820	–0.051	5.769	–9.627
319	82	416	–1.658	–2.654	6.316	3.545	–0.294	5.598	–9.527
319	83	276	–1.705	–2.951	7.277	4.954	1.382	6.115	–10.592
019/472	103	242	–1.298	–3.066	7.614	5.545	1.649	6.327	–11.099
019/472	105	277	–1.326	–3.055	7.375	5.045	1.221	6.325	–10.364
024/15/12	115	239	–1.028	–3.217	7.786	5.743	1.570	6.628	–10.870
106	84	265	–1.530	–3.160	7.555	5.307	1.584	6.528	–10.394
106	85	239	–1.004	–3.234	7.803	5.760	1.563	6.662	–10.836
106	86	300	–0.977	–2.961	7.146	4.678	0.476	6.149	–10.146
106	87	314	–1.032	–2.812	6.921	4.382	0.262	5.860	–10.227
	Max	566	–0.889	–2.226	9.805	8.532	5.130	9.442	–9.218
	Min	165	–1.820	–4.645	5.554	3.122	–1.564	4.808	–11.512

$$\log K_7 = -1 \times 10^{-7} T^3 + 0.0003T^2 - 0.2251T + 64.781, \quad (13)$$

$$\log K_8 = -6 \times 10^{-8} T^3 + 0.0002T^2 - 0.1783T + 48.175, \quad (14)$$

$$\log K_9 = 1 \times 10^{-9} T^3 - 2 \times 10^{-6}T^2 - 0.0001T + 1.0364, \quad (15)$$

$$\log K_{10} = 3 \times 10^{-8} T^3 - 6 \times 10^{-5}T^2 + 0.437T - 20.221, \quad (16)$$

$$\log K_{11} = -1 \times 10^{-7} T^3 + 0.0003T^2 - 0.224T + 64.905. \quad (17)$$

In all the above reactions, $a_{H_2O} = 1$ is used to calculate ratios of aqueous species such as $a_{SiO_{2(aq)}}$, a_{Na^+}/a_{H^+}, a_{K^+}/a_{H^+}, $a_{Ca^{2+}}/a_{H^+}^2$, $a_{Mg^{2+}}/a_{H^+}^2$ and $a_{Fe^{2+}}/a_{H^+}^2$ in the hydrothermal fluid from their corresponding reactions, i.e. eqs (6) through (11) for chlorite micro-domain. These are expressed as follows

$$\log(a_{SiO_{2(aq)}}) = \frac{1}{4}\{\log K_{10} - \log(a_{Clin}) + \log(a_{Tr})\}, \quad (18)$$

$$\log\left(\frac{a_{Ca^{2+}}}{a_{H^+}^2}\right) = \frac{1}{3}\{\log K_9 - \log(a_{Clin}) - 7\log(a_{SiO_{2(aq)}}) + \log(a_{Tr})\}, \quad (19)$$

$$\log\left(\frac{a_{Mg^{2+}}}{a^2_{H^+}}\right) = \frac{1}{5}\{\log K_{11} - \log(a_{SiO_{2(aq)}}) + \log(a_{Clin})\}, \quad (20)$$

$$\log\left(\frac{a_{K^+}}{a_{H^+}}\right) = \frac{1}{2}\left\{5\log\left(\frac{a_{Mg^{2+}}}{a^2_{H^+}}\right) - \log(a_{Clin}) - 3\log(a_{SiO_{2(aq)}}) - \log K_6\right\}, \quad (21)$$

$$\log\left(\frac{a_{Na^+}}{a_{H^+}}\right) = \frac{1}{2}\left\{5\log\left(\frac{a_{Mg^{2+}}}{a^2_{H^+}}\right) - \log(a_{Clin}) - 3\log(a_{SiO_{2(aq)}}) - \log K_7\right\}, \quad (22)$$

$$\log\left(\frac{a_{Fe^{2+}}}{a^2_{H^+}}\right) = \frac{1}{5}\left\{\log K_8 + 2\log(a_{Dph}) + 3\log(a_{SiO_{2(aq)}}) + 2\log\left(\frac{a_{Na^+}}{a_{H^+}}\right)\right\}, \quad (23)$$

The chlorite composition is used in the calculation of all the above parameters based on detailed mineralogical features observed in the micro-domain. Thermodynamic components used to represent the natural solid solutions in equilibrium calculations together with equations and data relating measured mineral compositions to activities of these components are given in Tables 3 and 4.

Activities of dissolved cations in hydrothermal fluids

Chemical mass transfer and thermodynamic modelling of mineral fluid equilibria is a quantitative simulation of rock alteration in natural hydrothermal systems based on thermodynamic database of minerals and aqueous fluids[20]. The generalized eq. (3) is used in the derivation of equations for activity relations of aqueous species with fluids in the Malanjkhand hydrothermal system. At constant pressure, temperature dependent kinetic equilibrium constant derived with respect to balanced chemical reactions 6 to 11. For chlorite micro-domain, eqs (6)–(11) are used in the calculation of ratios of aqueous species $a_{SiO_{2(aq)}}$, a_{Na^+}/a_{H^+}, a_{K^+}/a_{H^+}, $a_{Ca^{2+}}/a^2_{H^+}$, $a_{Mg^{2+}}/a^2_{H^+}$ and $a_{Fe^{2+}}/a^2_{H^+}$ respectively. However, observed phase relations and the above calculations indicate that K-feldspar in the chlorite micro-domain is characterized by the thermodynamic properties of microcline. Using thermodynamic data for sanidine as opposed to microcline in the other domain has only minor effects on the calculated activity ratios (D. Pandit, unpublished). In the chlorite micro-domain for assemblages of plagioclase and K-feldspar, the calculated $a_{SiO_{2(aq)}}$ is according to eq. (10). The calculated activity of silica during the chloritization in the estimated temperature range is given in Table 4. This corresponds to the mineral assemblage quartz, sanidine, albite, anorthite and fluid. Results imply that aqueous solutions in the Malanjkhand fossil geothermal system were supersaturated with α-quartz in the temperature range 110–400°C which is in equilibrium with chlorite (Figure 5 *a*).

Paleoproterozoic Malanjkhand hydrothermal system

Mass transfers in hydrothermal alteration systems are responsible for isochemical recrystallization of host rock and provide useful constrains on the activities of Na^+, K^+, Mg^{2+}, Ca^{2+} and Fe^{2+}-ions in the hydrothermal fluid[34]. Calculations presented above indicate systematic gradients in the activity ratios of alkali, alkaline-earth and iron-ions with respect to hydrogen-ions in the Malanjkhand hydrothermal system. In the biotite micro-domain calculated temperature varies from 236°C to 384°C in the Malanjkhand hydrothermal system at which biotites re-equilibrated with the internally evolved hydrothermal fluid[5]. According to Panigrahi and Mookherjee[35], composition of internally evolved hydrothermal fluid in the Malanjkhand hydrothermal system maintains equilibrium with quartz in the 140–380°C temperature range. However, calculated values of $a_{SiO_{2(aq)}}$ shown in Figure 5 *a* for chlorite mineral assemblages indicate supersaturation with respect to quartz. In chlorite micro-domain temperature varies in the 110–400°C range that corresponds to change in activity ratios of $a_{Ca^{2+}}/a^2_{H^+}$ and $a_{Mg^{2+}}/a^2_{H^+}$ at about 5–10 log units and 3–8 log units respectively (Figure 5 *b* and *c*). The activity of Fe^{2+} ion decreases with increasing temperature (Figure 5 *d*). Taking into account, the alternate calculations employed in generating data and reported in the figure, it is obvious that no discontinuities in the ratios a_{Na^+}/a_{H^+}, a_{K^+}/a_{H^+} and $a_{Ca^{2+}}/a^2_{H^+}$ are associated with the transition from chlorite to biotite mineral domains. However, the logarithms of a_{Na^+}/a_{H^+} and a_{K^+}/a_{H^+} for the chlorite micro-domain vary between 3 and 4 units within the range of temperature variation (Figure 5 *e* and *f*).

Discussion

Hydrothermal alteration is likely to be a more common phenomenon in the continental crust[36] and is responsible for the generation of many of the important ore deposits[5,37,38]. Hydrothermal fluids in plutonic settings are thought to circulate upward and outward from an igneous

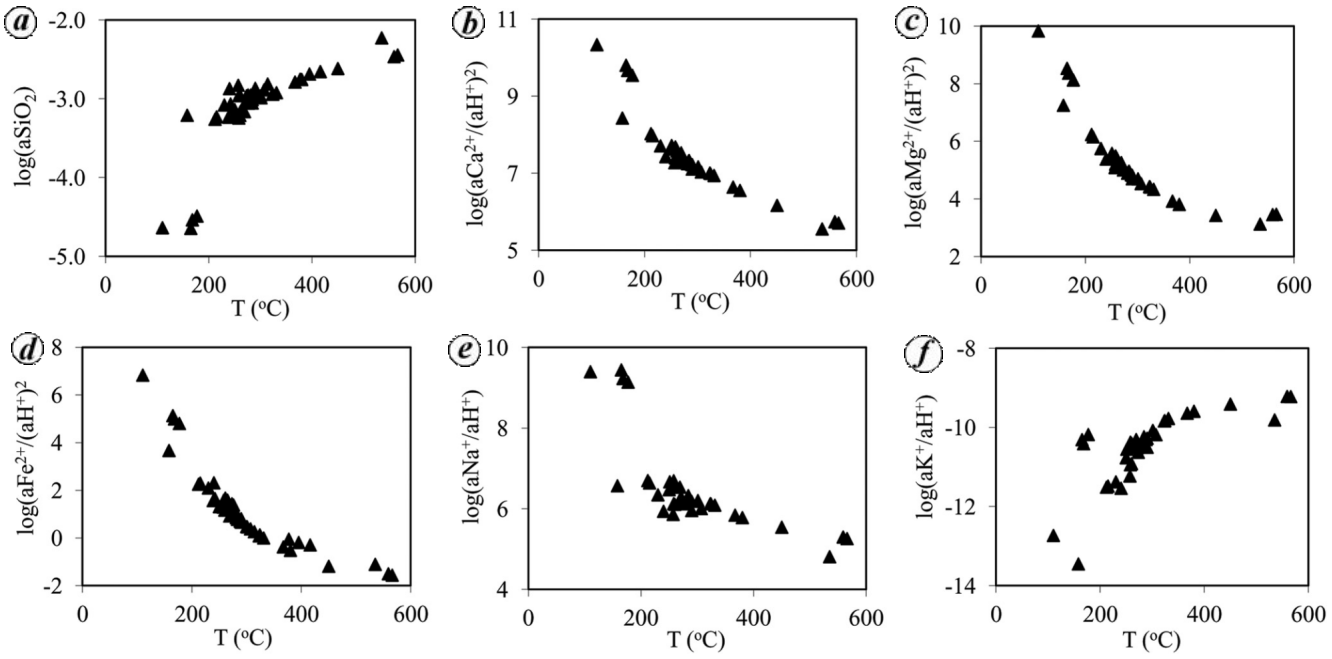

Figure 5. Calculated activities of aqueous species in hydrothermal fluid: (*a*) $a_{SiO_{2(aq)}}$, (*b*) $a_{Ca^{2+}}/a^2_{H^+}$, (*c*) $a_{Mg^{2+}}/a^2_{H^+}$, (*d*) $a_{Fe^{2+}}/a^2_{H^+}$, (*e*) a_{Na^+}/a_{H^+} and (*f*) a_{K^+}/a_{H^+} in equilibrium with chlorite plotted with respect to estimated temperature using the procedure of Vidal *et al.*[14].

intrusion at depth along a large-scale convective path. Porous and permeable host rocks allow this to happen more readily. Hydrothermal fluids also circulate along fractures and faults. Hydrothermal alteration of granitic plutons typically results in alteration of biotite and hornblende to chlorite. In MG, the activity ratios $a_{Ca^{2+}}/a^2_{H^+}$, $a_{Mg^{2+}}/a^2_{H^+}$, $a_{Fe^{2+}}/a^2_{H^+}$ and a_{Na^+}/a_{H^+} decrease with increase in alteration temperature (Figure 5 *b*–*e*), whereas ratios a_{K^+}/a_{H^+} increase (Figure 5*f*). This indicates that K^+ ions play a dominant role during chloritization, which is most probably released during the alteration of biotite under water-saturated conditions. Alteration of hornblende increased activities of Ca^{2+} ions in the hydrothermal fluid. In general, this process can be summarized as follows

$$5\text{Bio} + 3\text{An} + 3\text{SiO}_{2(aq)} + 4\text{H}_2\text{O} + 6\text{H}^+ = 3\text{Chl} + 5\text{Kf} + 3\text{Ca}^{2+} \quad (24)$$

$$10\text{Bio} + \text{Kln} + 7\text{H}_2\text{O} + 10\text{H}^+ = 6\text{Chl} + 14\text{SiO}_{2(aq)} + 10\text{K}^+, \quad (25)$$

$$\text{Hb} + \text{An} + 6\text{H}^+ = \text{Chl} + 7\text{SiO}_{2(aq)} + 3\text{Ca}^{2+}, \quad (26)$$

$$\text{Hb} + 2\text{Kf} + 6\text{H}^+ = \text{Chl} + 11\text{SiO}_{2(aq)} + 2\text{Ca}^{2+} + 2\text{K}^+, \quad (27)$$

Equations (24) and (25) indicate the formation of chlorite and K-feldspar because of alteration of biotite. Similarly, eqs (26) and (27) represent chloritization of hornblende in granite-related hydrothermal system. In MG, temperature estimated from mineral fluid equilibria calculations[5], fluid inclusions microthermometry[35] and sulphur-isotope composition[39] remarkably overlap in the range of 200–375°C. The temperature of chloritization ranges from 110°C to 400°C as calculated in this study, which is also consistent with the estimates from sulphides. Quantitative modelling of hydrothermal alteration processes such as chloritization can be used to develop and test geological models for ore formation and also can be applied for mineral exploration and resource assessment considering the zone of hydrothermal alteration which influenced the mineralization processes.

1. Bondi, M., Morten, L. and Rossi, P. L., Chlorites from Italian granitoid rocks. *Tschermaks Mineral. Petrogr. Mitt.*, 1976, **23**, 39–50.
2. Deer, W. A., Howie, R. A. and Zussman, J., *An Introduction to the Rock Forming Minerals*, Longman Group Limited, London, 1979, 2nd edn.
3. Bailey, S. W., Chlorites: structures and crystal chemistry. In *Hydrous Phyllosilicates* (ed. Bailey, S. W.), Reviews in Mineralogy, Mineralogical Society of America, Washington, DC, 1988, vol. 19, pp. 347–403.
4. Pandit, D. and Panigrahi, M. K., Comparative petrogenesis and tectonics of Palaeoproterozoic Malanjkhand and Dongargarh granitoids, Central India. *J. Asian Earth Sci.*, 2012, **50**, 14–26.
5. Panigrahi, M. K., Naik, R. K., Pandit, D. and Misra, K. C., Reconstructing physico-chemical parameters of hydrothermal mineralization at the Malanjkhand copper deposit, India from mineral chemistry of biotite, chlorite and epidote. *Geochem. J.*, 2008, **42**, 443–460.
6. Yedekar, D. B., Jain, S. C., Nair, K. K. K. and Dutta, K. K., The central Indian collision suture. *Geol. Soc. India Spec. Publ.*, 1990, **28**, 1–43.
7. Acharyya, S. K., The nature of Mesocroterozoic Central Indian Tectonic Zone with exhumed and reworked older granulites. *Gondwana Res.*, 2003, **6**, 197–214.
8. Jain, S. C. and Yedekar, D. B., A note on geological traverses in Nagpur–Balaghat–Bilaspur–Rajgarh area, Maharashtra and Madhya

Pradesh, for making the extension of Central Indian Shear/Suture Zone. *Rec. Geol. Surv. India*, 1989, **122**(170–171), 181–183.
9. Jain, S. C., Yedekar, D. B. and Nair, K. K. K., Central Indian shear zone: a major Precambrian crustal boundary. *J. Geol. Soc. India*, 1991, **37**, 521–532.
10. Mall, D. M., Reddy, P. R. and Mooney, W. D., Collision tectonics of the Central Indian Suture Zone as inferred from a deep seismic sounding study. *Tectonophysics*, 2008, **460**, 116–123.
11. Panigrahi, M. K., Bream, B. R., Misra, M. C. and Naik, R. K., Age of granitic activity associated with copper–molybdenum mineralization at Malanjkhand, Central India. *Miner. Deposita*, 2004, **39**, 670–677.
12. Panigrahi, M. K., Pandit, D. and Naik, R. K., Genesis of the granitoid affiliated Palaeoproterozoic copper–molybdenum deposit at Malanjkhand: a review of status. In *Magmatism, Tectonism and Mineralization* (ed. Kumar, S.), Macmillan Publisher India Ltd, 2009, pp. 265–292.
13. Panigrahi, M. K., Mookherjee, A., Pantulu, G. V. C. and Gopalan, K., Granitoids around the Malanjkhand copper deposit: types and age relationships. *Proc. Indian Acad. Sci.* (*Earth Planet. Sci.*), 1993, **102**, 399–413.
14. Vidal, O., Parra, T. and Trotet, F., A thermodynamic model for Fe–Mg aluminous chlorite using data from phase equilibrium experiments and natural pelitic assemblages in 100–600°C, 1–25 kbar *P–T* range. *Am. J. Sci.*, 2001, **301**, 557–592.
15. Fleming, P. D. and Fawcett, J. J., Upper stability of chlorite + quartz in the system MgO–FeO–Al_2O_3–SiO_2–H_2O at 2 kbar water pressure. *Am. Mineral.*, 1976, **61**, 1175–1193.
16. Chernosky, J. V., Berman, R. G. and Bryndzia, L. T., Stability, phase relations and thermodynamic properties of chlorite and serpentine group minerals. *Rev. Mineral. Geochem.*, 1988, **19**, 295–346.
17. Hey, M. H., A new review of the chlorites. *Mineral. Mag.*, 1954, **30**, 277–292.
18. Bird, D. K. and Norton, D. L., Theoretical prediction of phase relations among aqueous solutions and minerals: Salton Sea geothermal system. *Geochim. Cosmochim. Acta*, 1981, **45**, 1479–1493.
19. Holland, T. and Blundy, J., Non-ideal interactions in calc amphiboles and their bearing on amphibole–plagioclase thermometry. *Contrib. Mineral. Petrol.*, 1994, **116**, 433–447.
20. Heinrich, C. A., Walshe, J. L. and Harrold, B. P., Chemical mass transfer modeling of ore-forming hydrothermal systems: current practice and problems. *Ore Geol. Rev.*, 1996, **10**, 319–338.
21. Burnham, C. W., Holloway, J. R. and Davis, N. F., Thermodynamic properties of water to 1000°C and 10,000 bars. *Geol. Soc. Am. Spec. Paper*, 1969, **132**, 96.
22. Helgeson, H. C. and Kirkham, D. H., Theoretical prediction of the thermodynamic behavior of aqueous electrolytes at high pressures and temperatures. I. Summary of the thermodynamic/electrostatic properties of the solvent. *Am. J. Sci.*, 1974a, **274**, 1089–1198.
23. Helgeson, H. C. and Kirkham, D. H., Theoretical prediction of the thermodynamic behavior of aqueous electrolytes at high pressures and temperatures. II. Summary of the thermodynamic/electrostatic properties of the solvent. *Am. J. Sci.*, 1974b, **274**, 1199–1261.
24. Helgeson, H. C. and Kirkham, D. H., Theoretical prediction of the thermodynamic behavior of aqueous electrolytes at high pressures and temperatures. III. Summary of the thermodynamic/electrostatic properties of the solvent. *Am. J. Sci.*, 1976, **276**, 97–240.
25. Walther, J. V. and Helgeson, H. C., Calculation of the thermodynamic properties of aqueous silica and the solubility of quartz and its polymorphs at high pressures and temperature. *Am. J. Sci.*, 1977, **277**, 1315–1351.
26. Helgeson, H. C., Delany, J. M., Nesbitt, H. W. and Bird, D. K., Summary and critique of the thermodynamic properties of rock-forming minerals. *Am. J. Sci. A*, 1978, **278**A, 229.
27. Flowers, G. C., Correction of Holloway's (1977) adaptation of the modified Reich–Kong equation of state to calculation of the fugacities of molecular species in supercritical fluids of geological interest. *Contrib. Mineral. Petrol.*, 1979, **69**, 315–318.
28. Bird, D. K. and Helgeson, H. C., Chemical interaction of aqueous solutions with epidote–feldspar mineral assemblages in geologic system. I: thermodynamic analysis of phase relations in the system CaO–FeO–Fe_2O_3–Al_2O_3–SiO_2–H_2O–CO_2. *Am. J. Sci.*, 1980, **280**, 907–941.
29. MeKenzie, W. F. and Helgeson, H. C., Calculation of the dielectric constant of H_2O and the thermodynamic properties of aqueous species at temperatures to 900°C. *Geol. Soc. Am. Abstr. Progr.*, 1979, **11**, 476.
30. Helgeson, H. C., Prediction of the thermodynamic properties of electrolytes at high pressures and temperatures. In *Chemistry and Geochemistry of Solutions at High Temperatures and Pressures* (eds Wickman, F. and Rickard, D.), Royal Swedish Academy of Sciences, 1981.
31. Berman, R. G., Internally-consistent thermodynamic data for minerals in the system Na_2O–K_2O–CaO–MgO–FeO–Fe_2O_3–Al_2O_3–SiO_2–TiO_2–H_2O–H_2O–CO_2. *J. Petrol.*, 1988, **29**, 445–522.
32. Holland, T. J. B. and Powell, R., An internally-consistent thermodynamic dataset for phases of petrological interest. *J. Metamorphic Geol.*, 1998, **16**, 309–343.
33. Johnson, J. W., Oelkers, E. H. and Helgeson, H. C., SUPCRT92: a software package for calculating the standard molal thermodynamic properties of minerals, gases, aqueous species, and reactions from 1 to 5000 bar and 0 to 1000°C. *Comp. Geosci.*, 1992, **7**, 899–947.
34. Giggenbach, W. F., Mass transfer in hydrothermal alteration systems – a conceptual approach. *Geochim. Cosmochim. Acta*, 1984, **48**, 2693–2711.
35. Panigrahi, M. K. and Mookherjee, A., The Malanjkhand copper (+ molybdenum) deposit, India: mineralization from a low-temperature ore-fluid of granitoid affiliation. *Miner. Deposit.*, 1997, **32**, 133–148.
36. Pumper, O. and Putins, A., The complex hydrothermal history of granitic rocks: multiple feldspar replacement reactions under subsolidus conditions. *J. Petrol.*, 2010, **50**, 967–987.
37. Haynes, D. W., Cross, K. C., Bills, R. T. and Reed, M. H., Olympic Dam Ore genesis – a fluid-mixing model. *Econ. Geol.*, 1995, **90**, 281–307.
38. Barton, M. D. and Johnson, D. A., Evaporitic-source model for igneous-related Fe oxide – (REE–Cu–Au–U) mineralization. *Geology*, 1996, **24**, 259–262.
39. Panigrahi, M. K., Pandit, D., Naik, R. K. and Ishihara, S., Reconstruction of physicohemical environment of hydrothermal mineralization at Malanjkhand copper deposit, Central India: constraints from sulfur isotope ratios in pyrite, molybdenite and chalcopyrite. *Resour. Geol.*, 2013, **63**, 110–116.

ACKNOWLEDGEMENTS. I thank Dr S. Rajan, Director, National Centre for Antarctic and Océan Research, Goa for permission to publish this paper which contains some part of the author's Ph D thesis. Prof. Mruganka K. Panigrahi, IIT Kharagpur and Dr Rajesh K. Naik, Geological Survey of India (GSI), Kolkata are acknowledged for support in research during my tenure at IIT Kharagpur. CISR, New Delhi is acknowledged for grant of research fellowship and B. Chattopadhyay, S. K. Sengupta and S. Nandi, EPMA, GSI for EPMA analysis. I also thank R. Srinivasan for his critical suggestions on the MS.

Received 29 May 2013; revised accepted 4 December 2013